Supporting Information

Synthesis of Core-Shell Graphitic Carbon@Silica Nanospheres with Dual-Ordered Mesopores for Cancer-Targeted Photothermochemotherapy

Yi Wang[2], Kaiyuan Wang[4], Ren Zhang[2], Xingang Liu[2], Xueying Yan[4], Jianxin Wang[1], Ernst Wagner[1,3] and Rongqin Huang[1]*

[1] Department of Pharmaceutics, School of Pharmacy, Key Laboratory of Smart Drug Delivery, Ministry of Education, Fudan University, Shanghai 201203, China

[2] Center of Analysis and Measurement, Fudan University, Shanghai 200433, China

[3] Department of Pharmacy, Ludwig-Maximilians-Universitaet (LMU), Munich, 81377, Germany

[4] School of Pharmacy, Heilongjiang University of Chinese Medicine, Harbin 150040, China

Supporting Figures

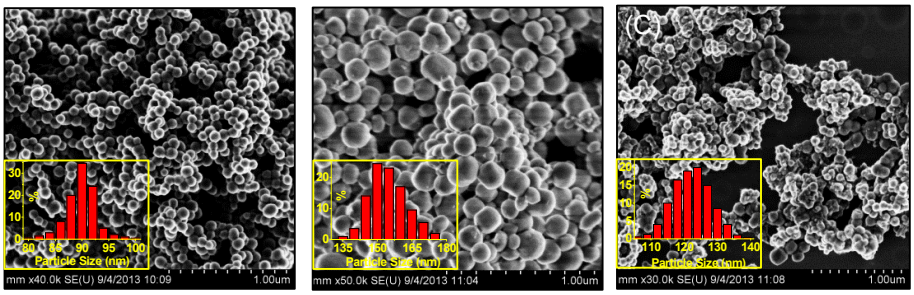

Figure S1. SEM images and corresponding particle size distribution curves (insets) of MCN (A), MCN@MS (B) and HMS (C).

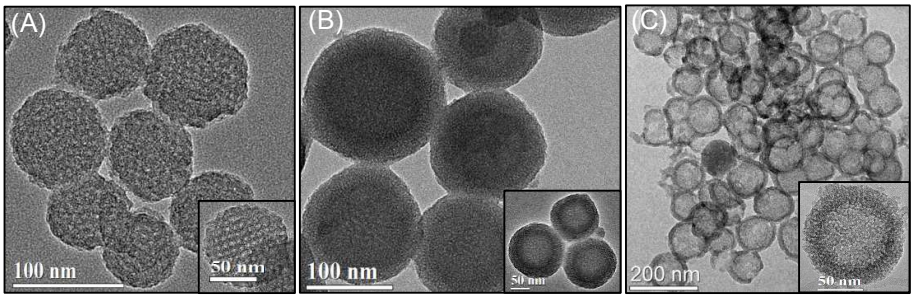

Figure S2. TEM and HRTEM (insets) images of MCN (A), MCN@MS (B) and HMS (C).

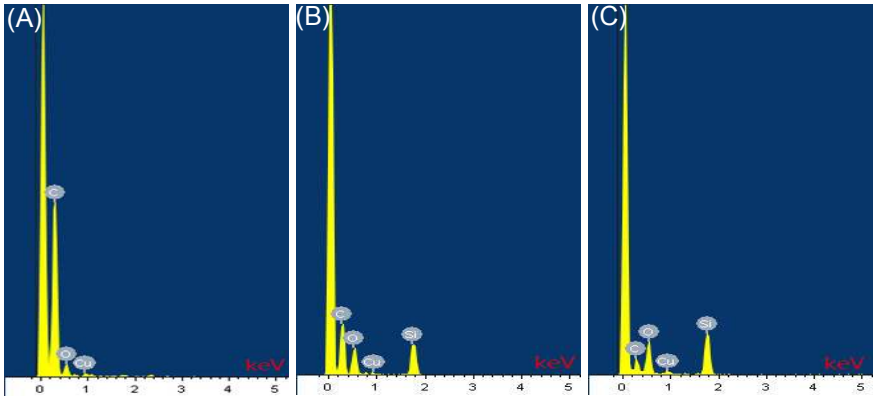

Figure S3. EDX patterns of MCN (A), MCN@MS (B) and HMS (C). The Cu and some few C elements came from the TEM grids with holey carbon supporting film.

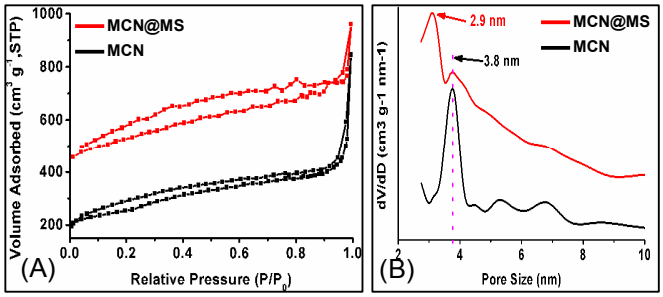

Figure S4. N_2 adsorption-desorption isotherm (A) and pore size distribution curve (B) of MCNs (Black) and MCN@MS (Red).

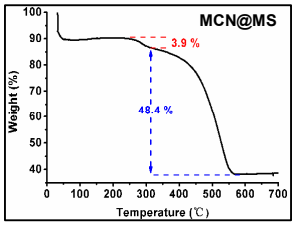

Figure S5. TGA curve of MCN@MS under oxygen atmosphere. The 3.9% weight loss was attributed to the dehydration by silanol condensation reaction,[1] while the 48.4% weight loss was caused by the decomposition of graphitic MCNs.

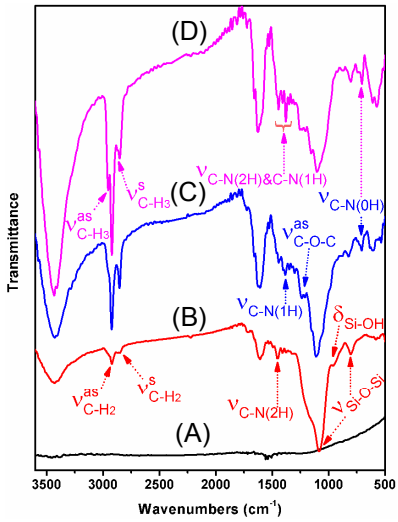

Figure S6. IR spectra of MCN (A), MCN@MS (B), MMP (C) and MMPS (D). MCN did not show any peaks since they were graphitic carbon with no infrared activity (A). Obvious peaks such as symmetrical stretching vibration (2843 cm^{-1}, $\nu^{s}_{C\text{-}H2}$) and asymmetrical stretching vibration (2915 cm^{-1}, $\nu^{as}_{C\text{-}H2}$) of C-H bonds in the methylene (-CH_2-), C-N stretching vibration of primary amide (1448 cm^{-1}, $\nu_{C\text{-}NH2}$), stretching vibration of Si-O-Si bond (symmetry: 802 cm^{-1}, $\nu^{s}_{Si\text{-}O\text{-}Si}$; asymmetry:1080 cm^{-1}, $\nu^{as}_{Si\text{-}O\text{-}Si}$) and bending vibration of Si-OH bond (961 cm^{-1}, $\delta_{Si\text{-}OH}$) emerged in sample MCN@MS, indicating that the amido-mesoporous silica was successfully modified on MCNs (B).[2] After PEGylation, the enhancement of C-H bonds stretching vibration in the methylene (-CH_2-) (2843 cm^{-1} & 2915 cm^{-1}, $\nu_{C\text{-}H2}$), the emergence of C-O-C bonds asymmetrical stretching vibration (1237 cm^{-1}, $\nu^{as}_{C\text{-}O\text{-}C}$), the transfer of C-N stretching vibration from primary amide (1448 cm^{-1}, $\nu_{C\text{-}NH2}$) to secondary amine (1380 cm^{-1}, $\nu_{C\text{-}NH}$) and tertiary amide (707 cm^{-1}, $\nu_{C\text{-}N}$) were clearly observed in MMP as compared with MCN@MS , proving the accomplished PEGylation (C). The SP13 conjugation was evidenced by two additional C-H bonds stretching vibrations in methyl (-CH_3) (2870 cm^{-1}, $\nu^{s}_{C\text{-}H3}$; 2954 cm^{-1}, $\nu^{as}_{C\text{-}H3}$), two much stronger C-H bonds stretching vibrations in the methylene (-CH_2-) (2843 cm^{-1}, $\nu^{s}_{C\text{-}H2}$; 2915 cm^{-1}, $\nu^{as}_{C\text{-}H2}$), and much more obvious C-N stretching vibration at 1300-1500 cm^{-1} & 700-750 cm^{-1} in sample MMPS (D), as compared with MMP.

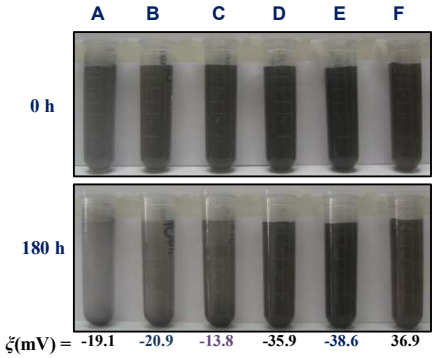

Figure S7. Dispersity of MCN (A), MCN@MS without amination (B), MCN@MS (C), MMP (D), MMPS (E) and MMPSD (F) solution. The prepared solutions were kept on standing for 180 h for the comparison. The zeta potentials of different nanoparticles were list below the pictures.

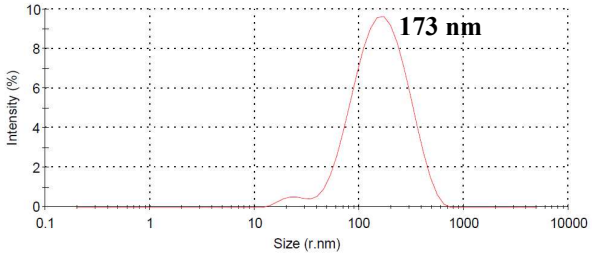

Figure S8. Particle size distribution curve of MMPSD measured by dynamic light scattering (DLS).

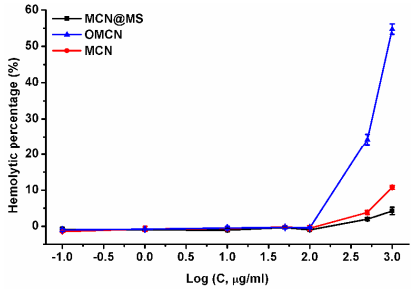

Figure S9. The hemolysis comparision of mesoporous silica coated and uncoated nanoparticles. Data were expressed as mean ± S.E.M. (n = 4).

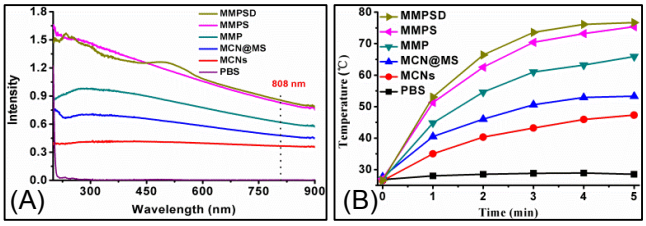

Figure S10. UV-vis spectra (A) and photothermal heating curves (B) (3.75 W cm^{-2} NIR at 808 nm) of different carriers with MCNs or MCN@MS concentration at 50 μg/ml.

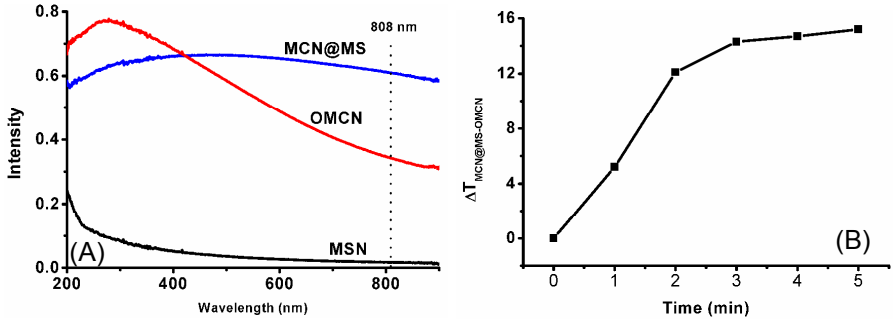

Figure S11. UV-vis absorption curves of samples with the same MCN (or MSN) concentration (A) and photothermal heating temperature differences (ΔT) between MCN@MS and OMCN solution with the same MCN concentration *via* NIR irradiation (3.75 W/cm^2, 808 nm) for different time periods (B).

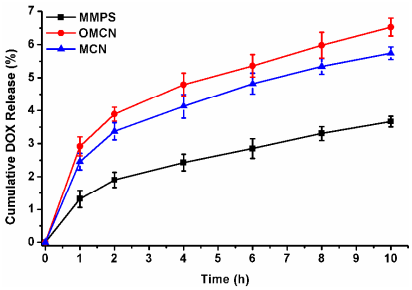

Figure S12. The cumulative DOX release profiles from different vectors under pH = 6.0.

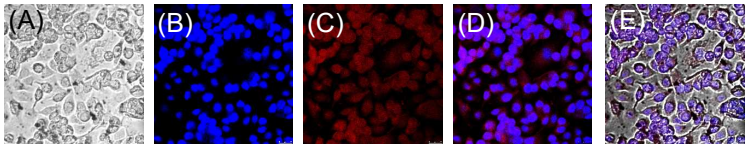

Figure S13 Intracellular localization of DOX within SK-BR-3 cells while incubated with MMPSD for 30 min. (A): bright field, (B): DAPI-stained nuclei, (C): DOX from MMPSD, (D): merged image of (B) and (C), (E): merged image of (A), (B) and (C). Bar = 50 μm.

Table S1

Textual Properties of Different Samples.

Sample	BET surface area ($m^2 g^{-1}$)	Total pore volume ($cm^3 g^{-1}$)	Unit cell (a_0)(nm)	Pore diameter (D)(nm)	Wall thickness (t) (nm)
MCNs	864	0.94	12.2	3.8	6.7
MCN@MS	518	0.71	5.6[a]	2.9[a]	2.7[a]
HMS	-	-	4.5	2.5	2.0

*a : The textual parameters of mesoporous silica coating, while the textual parameters of MCN was not obviously affected in MCN@MS.

*P6mm mesostructure (MCN@MS and HMS): $d_{100} = 2pi/q_{100}$, $a_0 = 2d_{100}/\sqrt{3}$, $t = a_0$ - D. pi=3.1415926.[3]

*$Im\bar{3}m$ mesostructure (MCN@MS and MCNs): $d_{110} = 2pi/q_{110}$, $a_0 = \sqrt{2}*d_{110}$, $t = \sqrt{3}*a_0/2$ - D. pi=3.1415926.[4]

Table S2

The Comparisons of Uncoated Nanopartilces (OMCN and MCN) with the Coated One (MMPS)

Samples	Sizes	Zeta Potentials	Temperature elevation compared to PBS[b]	drug loading capacity (mg/mg)	entrapment efficiency
MMPS	170 nm[a]	-38.6 mV	47.0 ℃	1.97 ± 0.28	79 %
MCN	90 nm	-19.1 mV	18.0 ℃	1.60 ± 0.22	64%
OMCN	90 nm	-43.0 mV	9.5 ℃	0.99 ± 0.25	40%

a: This size was measured by DLS. b: Irradiation for 5 minutes under 3.75 W cm^{-2} NIR at 808 nm with the same MCN concentration.

Table S3

IC_{50} (μg/ml) in SK-BR-3 Cells under Different Treatments and the Calculated CI.

MMPS	**MMPSD**	**MMPS+NIR**	**MMPSD+NIR**		**CI**
MCN@MS	DOX	MCN@MS	MCN@MS	DOX	**0.422**
3.50×10^7	92.61	18.03	5.10	10.05	

References

[1] Luan, Z. H., Fournier, J. A., Wooten, J. B., Miser, D. E. Preparation and Characterization of (3-Aminopropyl)triethoxysilane-Modified Mesoporous SBA-15 Silica Molecular Sieves. *Micropor. Mesopor. Mater.* **2005**, *83*, 150-158.

[2] Wang, Y.; Shi, W.; Song, W. S.; Wang, L.; Liu, X. G.; Chen, J.; Huang, R. Q. Tumor Cell Targeted Delivery by Specific Peptide-Modified Mesoporous Silica Nanoparticles. *J. Mater. Chem.* **2012**, *22*, 14608-14616.

[3] Wang, Y., Cui, D. M., Li, Q. Z. Synthesis, Characterization and Influence Parameters on the Overgrowth of Micro/Mesoporous Y-Zeolite-MCM-41 Composite Material under Acidic Conditions. *Micropor. Mesopor. Mater.* **2011**, *142*, 503-510.

[4] Ravikovitch, P. I., Neimark, A. V. Density Functional Theory of Adsorption in Spherical Cavities and Pore Size Characterization of Templated Nanoporous Silicas with Cubic and Three-Dimensional Hexagonal Structures. *Langmuir* **2002**, *18*, 1550-1560.